April 1, 2012

Dynamic reorganization of Eg5 in the mammalian spindle throughout mitosis requires dynein and TPX2

Alyssa Gable
Minhua Qui
Janel Titus
Sai Balchand
Nick P. Ferenz, et al.

Dynamic reorganization of Eg5 in the mammalian spindle throughout mitosis requires dynein and TPX2

Alyssa Gable[a,b], Minhua Qiu[c,d], Janel Titus[a,b], Sai Balchand[a,b], Nick P. Ferenz[a,b], Nan Ma[a], Elizabeth S. Collins[a], Carey Fagerstrom[a], Jennifer L. Ross[b,e], Ge Yang[c,d], and Patricia Wadsworth[a,b]

[a]Department of Biology and [b]Program in Molecular and Cellular Biology, University of Massachusetts Amherst, Amherst, MA 01003; [c]Department of Biomedical Engineering and [d]Lane Center for Computational Biology, Carnegie Mellon University, Pittsburgh, PA 15213; [e]Department of Physics, University of Massachusetts Amherst, Amherst, MA 01003

ABSTRACT **Kinesin-5 is an essential mitotic motor. However, how its spatial–temporal distribution is regulated in mitosis remains poorly understood. We expressed localization and affinity purification–tagged Eg5 from a mouse bacterial artificial chromosome (this construct was called mEg5) and found its distribution to be tightly regulated throughout mitosis. Fluorescence recovery after photobleaching analysis showed rapid Eg5 turnover throughout mitosis, which cannot be accounted for by microtubule turnover. Total internal reflection fluorescence microscopy and high-resolution, single-particle tracking revealed that mEg5 punctae on both astral and midzone microtubules rapidly bind and unbind. mEg5 punctae on midzone microtubules moved transiently both toward and away from spindle poles. In contrast, mEg5 punctae on astral microtubules moved transiently toward microtubule minus ends during early mitosis but switched to plus end–directed motion during anaphase. These observations explain the poleward accumulation of Eg5 in early mitosis and its redistribution in anaphase. Inhibition of dynein blocked mEg5 movement on astral microtubules, whereas depletion of the Eg5-binding protein TPX2 resulted in plus end–directed mEg5 movement. However, motion of Eg5 on midzone microtubules was not altered. Our results reveal differential and precise spatial and temporal regulation of Eg5 in the spindle mediated by dynein and TPX2.**

Monitoring Editor
Kerry S. Bloom
University of North Carolina

Received: Sep 28, 2011
Revised: Feb 3, 2012
Accepted: Feb 9, 2012

INTRODUCTION

Molecular motors play essential roles in mitosis, but how they are localized and regulated within the spindle during mitosis remains poorly understood. Eg5, a member of the kinesin-5 family, was one of the first mitotic motors identified and has subsequently been shown to be essential during mitosis in diverse cells (Le Guellec *et al.*, 1991; Hoyt *et al.*, 1992; Roof *et al.*, 1992; Sawin *et al.*, 1992; Heck *et al.*, 1993; Blangy *et al.*, 1995; Reddy and Day, 2001; Bannigan *et al.*, 2007). Structurally, Eg5 forms bipolar homotetramers, with motor domains located at each end of an elongated molecule (Cole *et al.*, 1994; Blangy *et al.*, 1995; Kashina *et al.*, 1996). This organization allows Eg5 to cross-link and slide adjacent parallel and antiparallel microtubules, a behavior that has been directly visualized in vitro (Kapitein *et al.*, 2005; van den Wildenberg *et al.*, 2008). Compared with other kinesin motor proteins, Eg5 is relatively slow and weakly processive (Sawin *et al.*, 1992; Cole *et al.*, 1994; Kwok *et al.*, 2006; Korneev *et al.*, 2007). Functional regulation of Eg5 may be mediated through its phosphorylation by cyclin-dependent kinase 1 in its tail domain (Blangy *et al.*, 1995), which increases Eg5 binding to microtubules in vitro and is required for localizing the motor to spindle microtubules in cells (Blangy *et al.*, 1995; Sawin and Mitchison, 1995; Cahu *et al.*, 2008). Additionally, Eg5 is regulated by the microtubule-associated protein TPX2, which localizes the motor to spindle microtubules and modulates motor activity (Ma *et al.*, 2011).

This article was published online ahead of print in MBoC in Press (http://www.molbiolcell.org/cgi/doi/10.1091/mbc.E11-09-0820) on February 15, 2012.

Address correspondence to: P. Wadsworth (patw@bio.umass.edu).

Abbreviations used: BAC, bacterial artificial chromosome; CC1, coiled coil-1; EGFP, enhanced GFP; FBS, fetal bovine serum; FRAP, fluorescence recovery after photobleaching; GFP, green fluorescent protein; HRP, horseradish peroxidase; IgG, immunoglobulin G; LAP, localization and affinity purification; ROI, region of interest; shRNA, short hairpin RNA; STLC, *S*-trityl-L-cysteine; TIRF, total internal reflection fluorescence.

Kinesin-5 motors are nearly universally required to generate outward forces for separation of spindle poles in early mitosis (Ferenz *et al.*, 2009). One example can be seen in inhibition of kinesin-5 motors in mammalian cells during spindle assembly, which results in a monopolar spindle phenotype (Mayer *et al.*, 1999). To generate outward forces, Eg5 requires overlapping antiparallel microtubules (Ferenz *et al.*, 2009). Eg5 localizes to spindle microtubules with enrichment near spindle poles (Sawin *et al.*, 1992; Blangy *et al.*, 1995; Sawin and Mitchison, 1995) and is also present on overlapping interzonal microtubules, consistent with the view that a critical site of Eg5 activity is on antiparallel microtubules (Sharp *et al.*, 1999; Cheerambathur *et al.*, 2008). The pole-separating activity of kinesin-5 is opposed by minus end–directed motors, which was first demonstrated by studies in fungi (Saunders and Hoyt, 1992) and subsequently in other cell types (Sawin *et al.*, 1992; Tanenbaum *et al.*, 2008; Ferenz *et al.*, 2010)

In *Xenopus* extract spindles, photoactivation experiments showed that kinesin-5 motors are static in the spindle midzone and are transported poleward in the half-spindle (midway between the chromosomes and pole) in a dynein/dynactin-dependent manner (Uteng *et al.*, 2008). Similarly, kinesin-5–green fluorescent protein (GFP) in *Drosophila* embryo spindles also provides evidence for motor transport in the spindle; whereas only a minor fraction of motors is static (Cheerambathur *et al.*, 2008). Static motors in the midzone could result if plus end–directed motors engaged on antiparallel microtubules stopped walking under load (Korneev *et al.*, 2007). Alternatively, static motor behavior could result if plus end–directed motor activity was matched by minus end–directed microtubule flux at a similar rate or if motors were linked to a static matrix (Kapoor and Mitchison, 2001; Tsai *et al.*, 2006; Uteng *et al.*, 2008).

To examine Eg5 behavior in a mammalian system, we generated cells expressing mouse Eg5 from a bacterial artificial chromosome (BAC) such that the protein was expressed under endogenous regulation to best match expression of native Eg5. This construct was called mEg5. We confirmed that mEg5 is functionally competent and forms heterotetramers with native Eg5. Using fluorescence recovery after photobleaching (FRAP), we found that Eg5 turns over rapidly in the spindle at a rate faster than can be accounted for by microtubule dynamics. To examine Eg5 spatial–temporal dynamics at a higher resolution, we used total internal reflection fluorescence (TIRF) microscopy and single-particle tracking (Yang *et al.*, 2008) to follow the behavior of individual Eg5 punctae on astral and midzone microtubules. Individual punctae are highly dynamic, with the majority having dwell times <200 ms. On astral microtubules, Eg5 punctae showed transient directed motion toward the minus ends in early mitosis but switched to slower plus end–directed motion later in mitosis. In contrast, Eg5 punctae moved transiently both toward and away from spindle poles on microtubules in the spindle midzone, in which static Eg5 punctae were not detected. Inhibition of dynein/dynactin with the coiled coil-1 (CC1) fragment of p150 blocked the minus end–directed movement of Eg5. In addition, depletion of the microtubule-associated protein TPX2 resulted in switching of Eg5 from minus end–directed to plus end–directed movement on astral microtubules, suggesting that TPX2 is required to couple Eg5 to dynein. However, Eg5 movement on interzonal microtubules was not affected. Together, our results demonstrate that Eg5 dynamics within the mammalian spindle are region-specific, that the motor reorganizes at different stages of mitosis, and that its dynamic reorganization is mediated by dynein and TPX2.

RESULTS

mEg5 is functionally competent

To examine the distribution and turnover of Eg5 in mammalian cells, we generated a clonal pig epithelial LLC-Pk1 cell line expressing mouse Eg5 from a BAC (Kittler *et al.*, 2005). This method allows the gene of interest to be expressed from the native locus with all regulatory elements, including the endogenous promoter. A localization and affinity purification (LAP) tag encoding enhanced GFP and S-peptide was added to the C-terminus of mouse Eg5 (Cheeseman and Desai, 2005; Poser *et al.*, 2008).

We evaluated mEg5 expression, localization, and function in the clonal cell line. mEg5 localization in mitotic cells was indistinguishable from previous results obtained using either Eg5-GFP expressed from a cDNA-containing plasmid or immunolocalization with antibodies directed against Eg5, and the expressed mEg5 colocalized with total Eg5 in these cells (Figure 1A and Supplemental Figure S1A; Sawin *et al.*, 1992; Blangy *et al.*, 1995). The mitotic index of the cell line was indistinguishable from the parental population (Figure S1B). To determine whether mEg5 forms heterotetramers with endogenous pig Eg5, which would be expected for a functional protein, we recovered mEg5 from cell lysates using S-peptide beads and found that both mEg5 and endogenous Eg5 were recovered (Figure 1B), suggesting the formation of heterotetramers.

To further test the functionality of mEg5, we examined whether mEg5 could rescue the loss of endogenous Eg5. First, we confirmed that inhibition of Eg5 with monastrol resulted in monopolar spindles in parental and mEg5 cells (Figure 1C). Next we designed short hairpin RNAs (shRNAs) to specifically target the pig sequence. However, we could not obtain knockdown of endogenous Eg5 without depleting mEg5 as well. To overcome this limitation, we established shRNA treatment conditions that resulted in depletion of ~50% of total Eg5 (Figure 1D); under these conditions, we found that ~80% of mEg5 cell spindles were bipolar (Figure 1C), cells progressed through mitosis without detectable abnormalities, and the distribution of mEg5 was unchanged (Figure 1E). Treatment for 48 h with this shRNA sequence resulted in monopolar spindle formation. Because the cell line expresses equivalent levels of mouse and pig Eg5, and each protein is similarly reduced following 24-h shRNA treatment (Figure 1D), this result demonstrates that mEg5 is functional in LLC-Pk1 cells under these conditions. Because overexpression of Eg5 (Vanneste *et al.*, 2009) or expression of mEg5 and pig Eg5 had no detectable mitotic defects, we used cells expressing mEg5 with and without RNA interference treatment for our experiments and obtained identical results under both conditions, further confirming our finding that mEg5 is functional in LLC-Pk1 cells.

Distribution of mEg5 in mitotic cells

To examine the distribution of mEg5 and microtubules throughout mitosis, we transfected cells expressing mEg5 with mCherry-tubulin and created a clonal cell line. In prophase cells (Figure 2A), mEg5 was detected along astral microtubules and accumulated at each centrosome, forming a bright ring that persisted throughout mitosis, consistent with a previous report (Vanneste *et al.*, 2009). Following nuclear envelope breakdown, mEg5 was observed along microtubules in the forming spindle with an enrichment of mEg5 at the poleward ends of spindle microtubules (Figure 2A). In early anaphase, mEg5 remained associated with shortening microtubules in the half-spindle and around each centrosome, but was barely detectable on midzone microtubules between the separating chromosomes. In late anaphase, however, mEg5 appeared in the midzone with a region of reduced fluorescence in the center of the

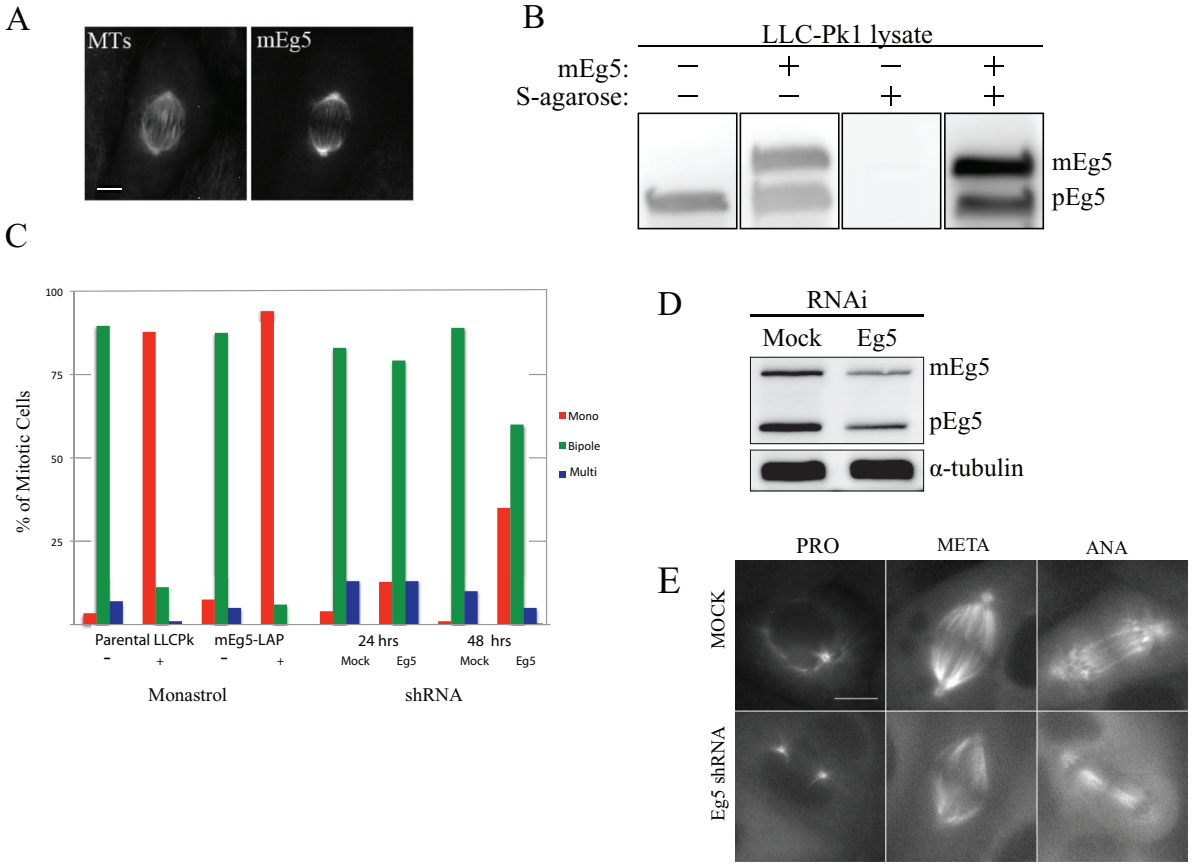

FIGURE 1: Validation of functional competence of mEg5. (A) Distribution of mEg5 and microtubules in a metaphase LLC-Pk1 cell. (B) mEg5 interacts with endogenous Eg5; Western blot of cell extracts and recovered protein stained for Eg5. Equivalent concentrations of parental and mEg5 cell lysate were added to S-beads and the S-bead pellet was resuspended in one-fifth the volume of the lysate; equal volumes were loaded for all lanes. (C) Percentage of monopolar spindles in parental or mEg5 LLC-Pk1 cells following treatment with monastrol or shRNA targeting Eg5. Number of cells counted: parental with (87 cells) and without (123 cells) monastrol; mEg5 with (80 cells) and without (100 cells) monastrol; mock siRNA at 24 (100 cells) and 48 (101 cells) h; Eg5 siRNA at 24 (101 cells) and 48 (105 cells) h. (D) Western blot showing level of endogenous and mouse Eg5 in parental cells and cells treated with shRNA for 24 h; tubulin loading control (bottom). (E) Distribution of mEg5 in mock treated (top) or cells treated with shRNA targeting Eg5 for 24 h (bottom). Scale bars: 10 μm.

anaphase midzone (Supplemental Movie S1 and Figure 2A). Only diffuse fluorescence of mEg5 was observed following treatment of cells with nocodazole, demonstrating that spindle localization of mEg5 requires intact microtubules (Figure S1C).

To quantify mEg5 distribution in the spindle, we measured mEg5 and tubulin fluorescence near the spindle poles and in the center of the midzone and determined the relative enrichment of each protein at the spindle poles. In prometaphase and metaphase cells, the enrichment of Eg5 at spindle poles was approximately threefold greater than that of microtubules. In early anaphase cells, mEg5 was also enriched at the spindle poles relative to the midzone. The extent of poleward enrichment decreased in late anaphase, as Eg5 accumulated on midzone microtubules ($p = 0.056$ and 0.051 for late anaphase compared with metaphase and early anaphase, respectively; Figure 2B).

In summary, these observations show that the localization of mEg5 is spatially and temporally regulated throughout mitosis in mammalian cells. The motor is distributed along microtubules in prometaphase and metaphase and is enriched relative to tubulin near spindle poles. In late anaphase, mEg5 relocalizes to the midzone region.

Rapid turnover of mEg5 in the mammalian spindle

To understand the source of reorganization of Eg5 spatial distribution at different stages of mitosis, we started by examining the dynamic turnover of mEg5. We performed FRAP in the half-spindle in prometaphase, metaphase, and anaphase cells; at the centrosome in prophase cells; and in the midzone region between the separating chromosomes of mid- to late anaphase cells. FRAP measurements in the midzone of prometaphase and metaphase cells were not obtainable, due to low fluorescence signal in this region (Figure 2A). In the half-spindle of prometaphase and metaphase cells, recovery was extremely rapid (half-times of 5.0 ± 2.0 and 6.0 ± 4.2 s, respectively), and a high percentage of the bleached fluorescence was recovered (Figure 3, A and B, Table 1, and Movie S2). The dynamics of mEg5 at the centrosome in prophase cells was similarly rapid (7.3 ± 4.3 s). In late anaphase cells, the dynamics of mEg5 on midzone microtubules was even more rapid than mEg5 in the half-spindle (Table 1), which could result from a decrease in Eg5 phosphorylation as cells exit mitosis (Blangy *et al.*, 1997; Cahu *et al.*, 2008). Statistically identical results ($t_{1/2}$ of 5.5 ± 1.4 and 7.3 ± 1.4 in prometaphase and metaphase, respectively) were obtained using cells treated with shRNA to reduce

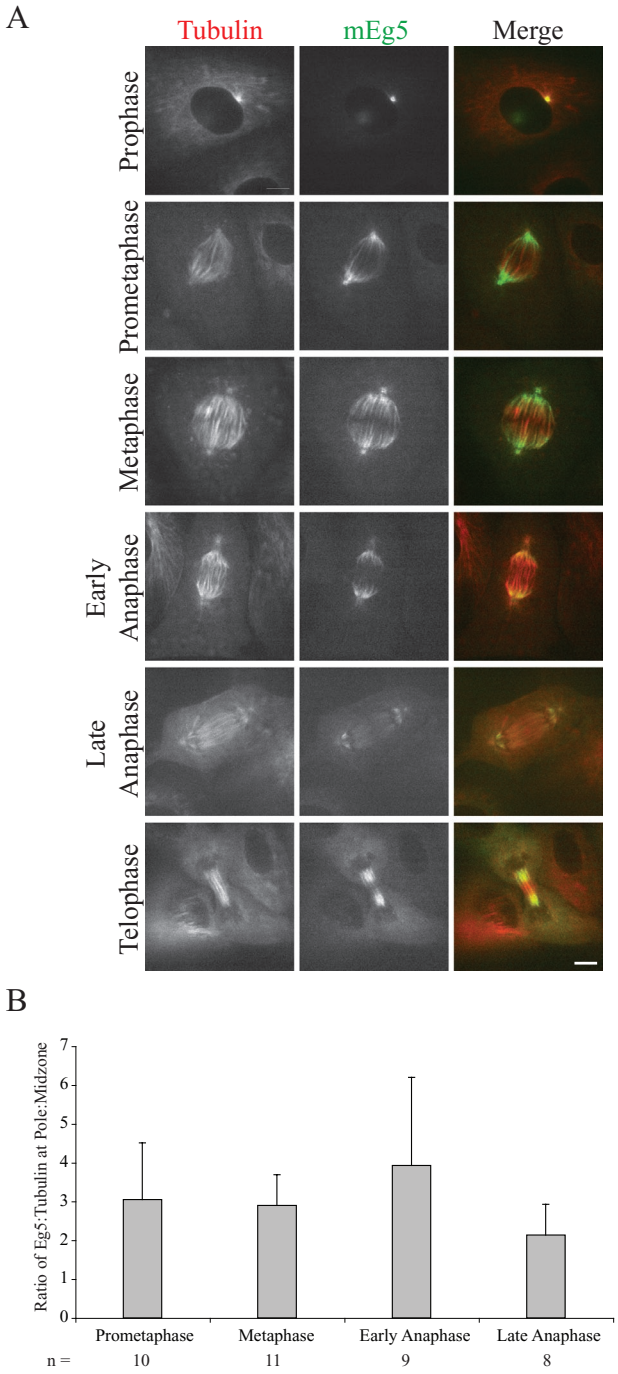

FIGURE 2: Distribution of mEg5 in the mammalian mitotic spindle. (A) Confocal images of cells expressing mEg5 (green) and mCherry-tubulin (red) and (B) quantification of Eg5 enrichment at spindle poles. Bars show SD. *t* test comparing late anaphase with metaphase and early anaphase, p = 0.056 and 0.051, respectively. Scale bar: 10 μm.

total Eg5 by ~50%; this was expected, as mEg5 is functionally competent.

We compared the turnover of mEg5 with that of GFP-tubulin, also measured using FRAP. The half-time for tubulin turnover in the half-spindle of prometaphase and metaphase cells and in the midzone of late anaphase cells was substantially slower than the turnover of mEg5 at the corresponding locations (Table 1). These results demonstrate that the dynamics of microtubules cannot account for the rapid exchange of mEg5 on spindle microtubules. To examine this further, we measured turnover of mEg5 in cells treated with paclitaxel to stabilize microtubules and block plus-end growth (Amin-Hanjani and Wadsworth, 1991; Yvon *et al.*, 1999). Under these conditions, turnover of mEg5 was indistinguishable from that measured in untreated cells, further indicating that microtubule assembly dynamics cannot account for the turnover of Eg5 (Table 1).

These results show that mEg5 is highly dynamic at all stages of mitosis, that the rate of turnover of mEg5 is faster than that of spindle microtubules, and that inhibition of microtubule turnover does not alter mEg5 dynamic turnover. On the basis of these results, we conclude that the dynamics of microtubules cannot account for the rapid turnover of mEg5. Our results are consistent with observations in *Drosophila* embryo spindles, in which rapid and nearly complete turnover of kinesin-5 was observed, although in these cells microtubules and motors turn over at a similar, rapid rate (Cheerambathur *et al.*, 2008). Using FRAP, we did not detect directed motion of mEg5, as observed in *Xenopus* and *Drosophila* spindles. We reason that an approach with higher spatial and temporal resolution is needed to examine the behavior of individual mEg5 in LLC-Pk1 cells.

Directed motion of mEg5 visualized by TIRF microscopy

To obtain high-resolution information about the dynamics of Eg5 in LLC-Pk1 cells, we used TIRF microscopy. In LLC-Pk1 cells, which remain flat throughout mitosis, deconvolution imaging shows that the overlapping microtubules in the midregion of the spindle are located sufficiently close to the cell periphery for TIRF imaging (Figures 4 and S2A; Mastronarde *et al.*, 1993). Microtubules in the half-spindle could not be imaged by this method. However, astral microtubules that radiate from each centrosome (Rusan and Wadsworth, 2005) could be detected by TIRF. For these experiments, we first imaged the spindle in cells expressing mEg5 using wide-field fluorescence microscopy to determine the location of the microtubules in the spindle. We then acquired time-lapse images of mEg5 in the same spindle in TIRF (Figure 4). Standard deviation intensity projections of time-lapse TIRF image sequences (Cai *et al.*, 2007) show that punctae of mEg5 are arranged in linear tracks, consistent with mEg5 binding and moving directionally along microtubules (Figure 4A). Also consistent with this, the linear pattern of fluorescent punctae was abolished when cells were treated with nocodazole to disassemble microtubules, which is expected if Eg5 motors associate with and transport along microtubules. Similarly, following inhibition of Eg5 with *S*-trityl-L-cysteine (STLC), linear tracks of punctae could not be detected in maximum intensity projections (Figure S3, A and B).

The time-lapse sequences revealed that individual punctae were very dynamic. To quantify the behavior of mEg5 punctae on astral and spindle microtubules, we used an automated software for high-resolution, single-particle tracking (Yang *et al.*, 2008). For astral microtubules, we were able to assign the polarity of the microtubule tracks from the maximum projection images using the wide-field images as guides (Figure 4B). In the midzone, microtubule polarity could not be assigned by visual inspection, so only the magnitude of the displacement of the punctae was considered in analysis (see *Materials and Methods*). From the image sequences, the dwell time of individual punctae and the mean displacement of punctae that remained on a microtubule for a given interval were determined; punctae that remained in the time-lapse sequence for less than two frames were excluded from motion calculation (see *Materials and Methods*). The dwell time of mEg5 punctae on both astral and interzonal microtubules was very short, typically at a few hundred milliseconds (Figure 4C and Supplemental Table S1).

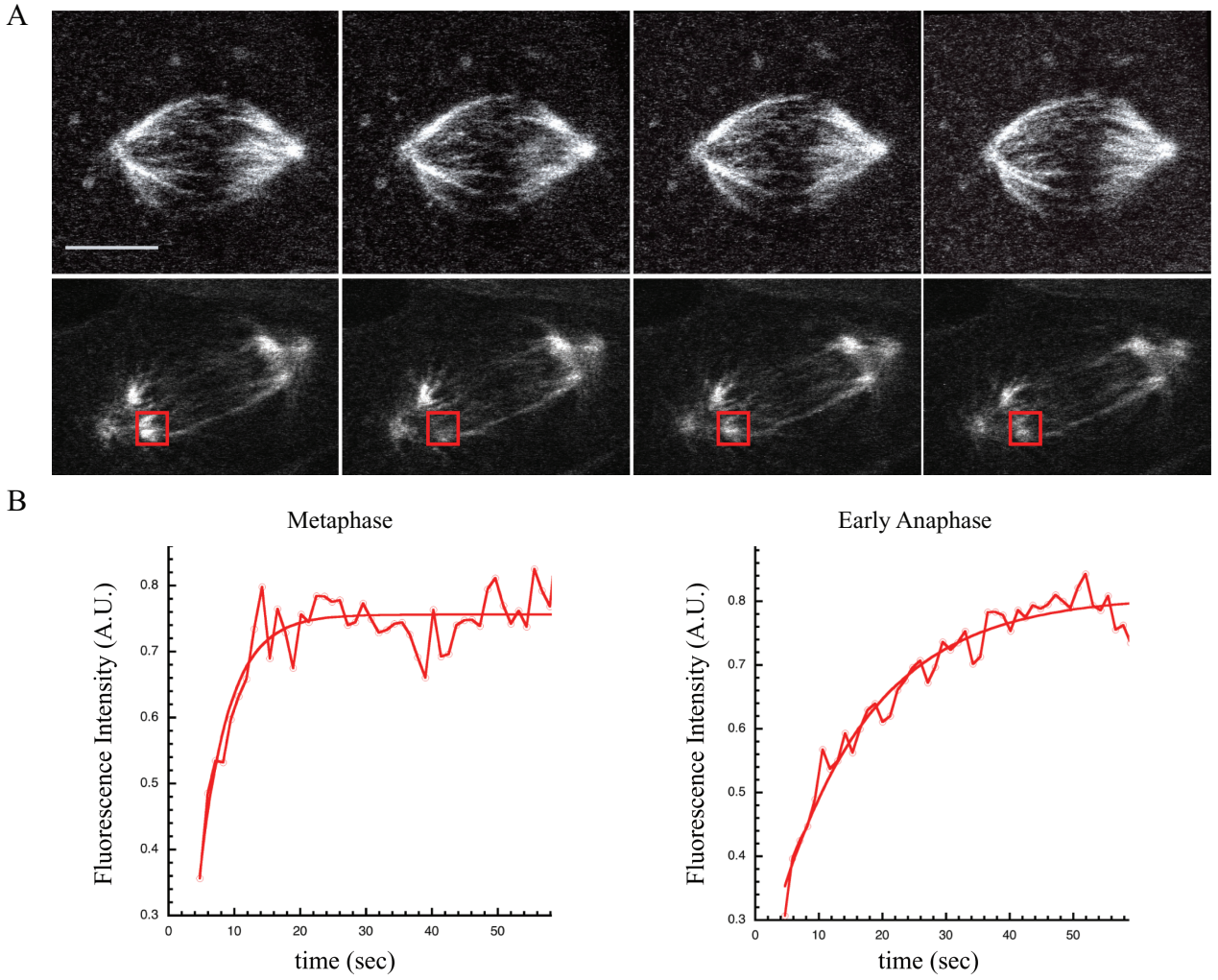

FIGURE 3: Rapid turnover of mEg5 in mitotic LLC-Pk1 cells. (A) Representative examples of FRAP of a metaphase and anaphase cell; red boxes show the bleached regions. (B) Recovery curves for the cells in (A). Scale bar: 10 μm.

On astral microtubules, the motion of punctae was diffusive in prophase but became minus end–directed in prometaphase and metaphase (Figure 5, A and C). Because astral microtubules do not undergo detectable microtubule flux, the motions we detected must result from motors moving on microtubules. In early anaphase, punctae on astral microtubules reversed direction and moved

		Prophase	Prometaphase	Metaphase	Early anaphase	Late anaphase
Half-time(s)[a]	Eg5	7.3 ± 4.3	5.0 ± 2.0	6.0 ± 4.2	8.8 ± 4.00	3.2 ± 1.1
		n = 6	n = 11	n = 17	n = 5	n = 12
	Eg5 + paclitaxel	—	5.6 ± 2.16	7.1 ± 6.22	9.2 ± 3.98	—
			n = 5	n = 12	n = 12	
	α-Tubulin	—	15.7 ± 6.60	19.9 ± 13.3	15.2 ± 5.8	9.3 ± 4.0
			n = 8	n = 8	n = 5	n = 3
Percent recovery[b]	Eg5	86.6 ± 20.6	103.8 ± 18.5	85.1 ± 23.5	91.8 ± 11.4	87.1 ± 15.5
	Eg5 + paclitaxel	—	89.4 ± 13.0	90.0 ± 20.7	86.1 ± 18.1	—
	α-Tubulin	—	86.4 ± 14.4	94.8 ± 16.9	63.8 ± 22.1	75.0 ± 21.6

The sample numbers (n) for recovery measurements are the same as the corresponding half-time measurements. —, Not determined.
[a]Half-time of Eg5 is significantly different from tubulin at prometaphase, metaphase, and late anaphase ($p \leq 0.01$). Half-time of Eg5 + placitaxel is significantly different from tubulin at prometaphase and metaphase ($p \leq 0.01$) and early anaphase ($p \leq 0.05$). Half-time of Eg5 in late anaphase is significantly different from Eg5 prophase and early anaphase ($p \leq 0.05$) and prometaphase and metaphase ($p \leq 0.01$).
[b]Percent recovery of Eg5 is significantly different from tubulin at early anaphase ($p \leq 0.05$) and prometaphase ($p \leq 0.05$).

TABLE 1: Eg5 turnover during mitosis in mammalian LLC-Pk1 cells.

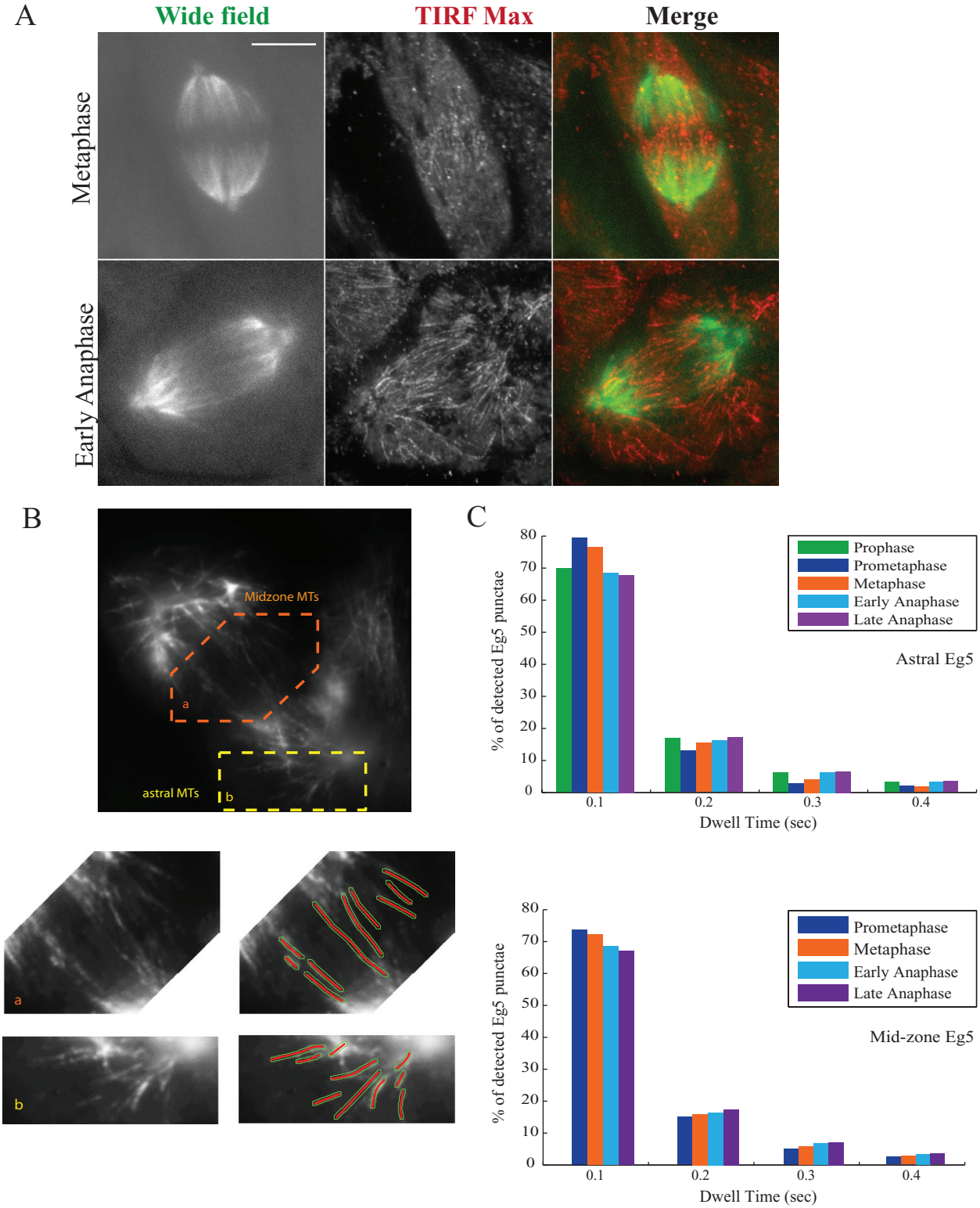

FIGURE 4: Single-particle tracking of Eg5 punctae in LLC-Pk1 cells. (A) Representative wide-field and SD intensity projections of TIRF time-lapse images (TIRF Max); merged on the right. Scale bar: 10 μm. (B) Identification of microtubules for TIRF analysis; midzone microtubules are located in the central region of the spindle (a), astral microtubules extend from each spindle pole (b). (C) Dwell time of Eg5 on astral and midzone microtubules.

toward microtubule plus ends (Figure 5, A and C). In late anaphase, punctae on astral microtubules switched again to diffusive behavior (Figure 5, A and C), indicating that Eg5 behavior is regulated as cells exit mitosis.

Next we tracked the behavior of punctae on microtubules in the spindle midzone in prometaphase and metaphase, where mEg5 was barely detectable using conventional confocal fluorescence microscopy (Figure 2A), and on midzone microtubules in anaphase

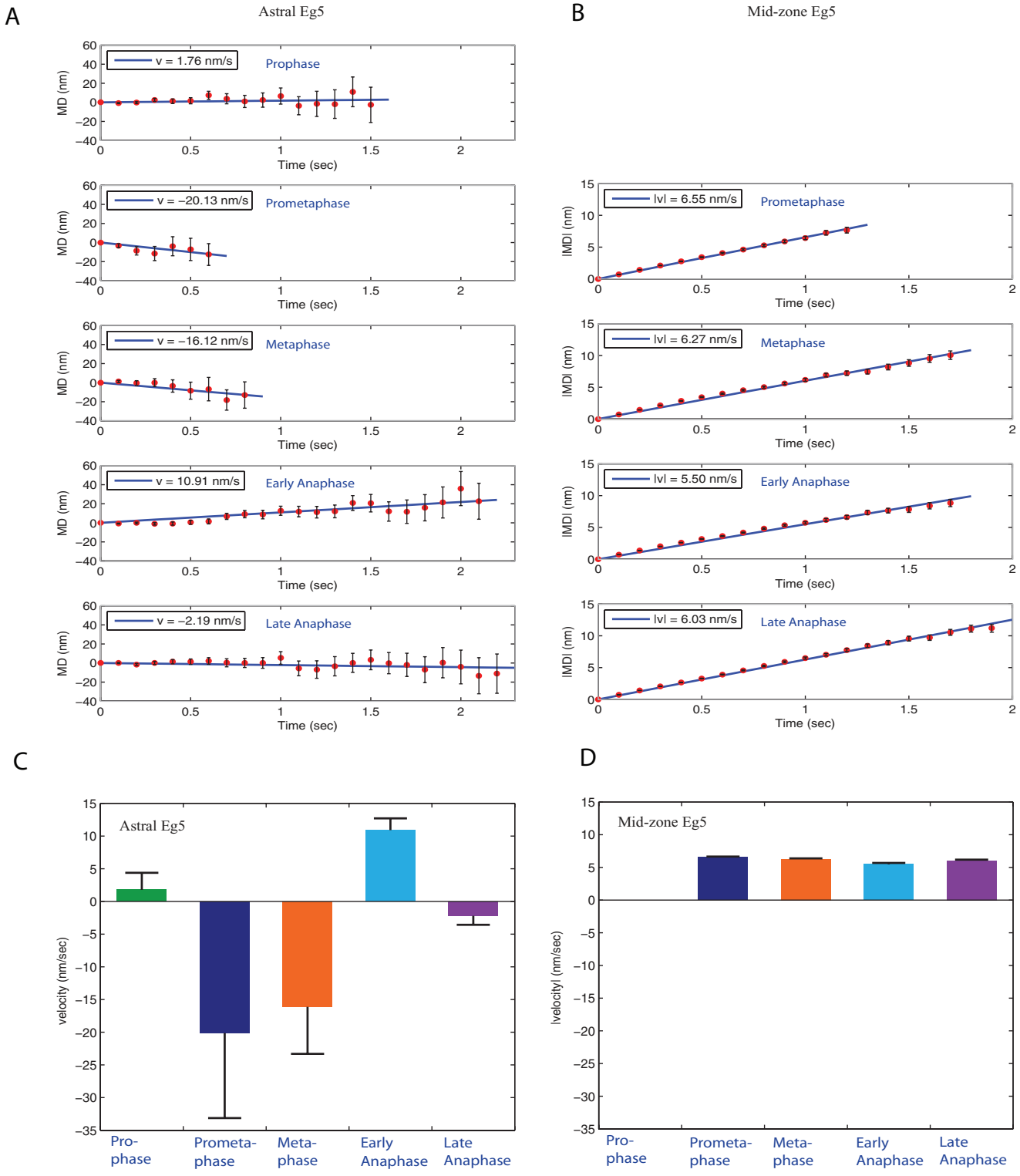

FIGURE 5: Motility of mEg5 on astral and midzone microtubules. Mean displacement fitting to achieve the velocities of astral and midzone Eg5 punctae (A and B) and velocities of astral and midzone Eg5 punctae at different phases (C and D). On astral microtubules (A and C), punctae move toward the microtubule minus end (negative velocity) during prometaphase and metaphase, switching to plus end–directed motion in early anaphase. For midzone microtubules (B and D), only the magnitude of displacement was analyzed, because microtubule polarity is not known. (A and B) Error bars show SE of the mean; in bar plots (C and D), velocities are plotted in mean ± 95% confidence interval of the estimated velocities.

cells. In prometaphase cells, mEg5 on midzone microtubules was very dynamic and moved bidirectionally, with average velocity of 6.55 nm/s. Similar motion was observed in metaphase and anaphase (Figure 5, B and D). A possible explanation for the slow velocity of Eg5 on midzone microtubules is that velocity is reduced under load as motor heads at both ends of the heterotetramer engage and walk on antiparallel microtubules (Korneev *et al.*, 2007).

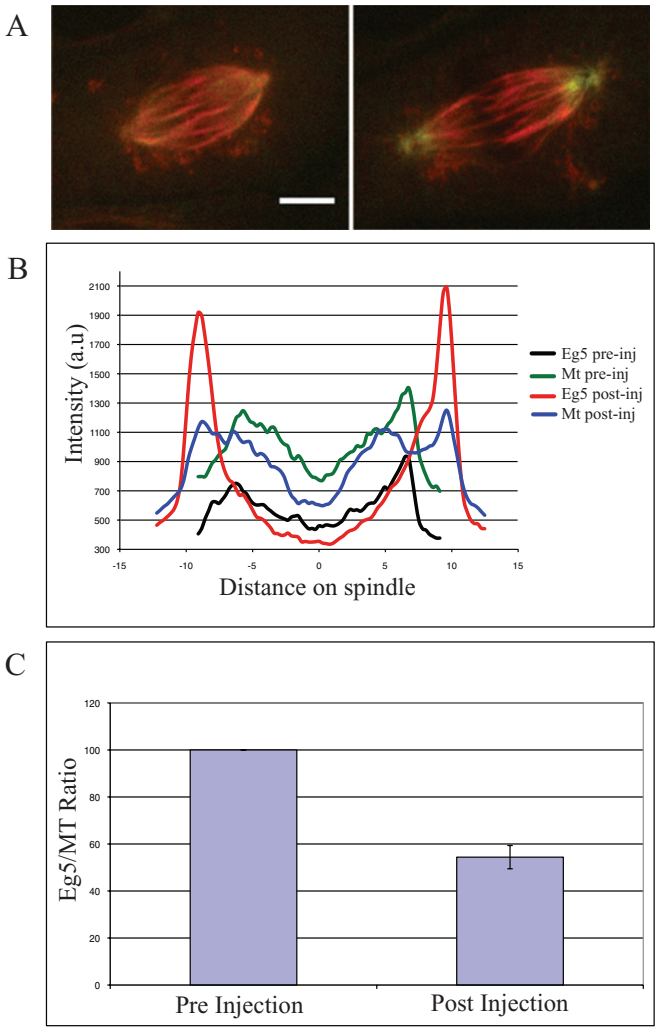

FIGURE 6: Dynein contributes to Eg5 localization to spindle microtubules. (A) Distribution of mEg5 and microtubules in a metaphase LLC-Pk1 cell prior to and 30 min postinjection with CC1. Green: mEg5; red: mCherry-tubulin. (B) Line scans along the pole-to-pole axis of the cell shown in (A). (C) Ratio of Eg5 to tubulin fluorescence. n = 5 cells; error bar = SD. Scale bar: 5 μm.

Dynamic reorganization of Eg5 in the spindle is mediated by dynein and TPX2

To understand how the direction of Eg5 transport in the spindle is regulated, we inhibited the dynein–dynactin interaction using the CC1 fragment of p150 (Quintyne *et al.*, 1999; King *et al.*, 2003; Ferenz *et al.*, 2009). As expected, microinjection of CC1 into mitotic cells resulted in bent and buckled microtubules in the spindle midzone and spindle elongation (Ferenz *et al.*, 2009). Using cells expressing mEg5 and mCherry-tubulin, we found that the distribution of mEg5 was altered following CC1 injection (Figure 6A). Line scans along the spindle axis showed that mEg5 fluorescence was reduced in the half-spindle and increased at spindle poles (Figure 6B). The ratio of Eg5 to tubulin fluorescence in the half-spindle was significantly decreased 30 min following injection of CC1 (Figure 6C), demonstrating that dynein activity is important for Eg5 localization to spindle microtubules (Uteng *et al.*, 2008).

We next examined the behavior of mEg5 punctae on astral and midzone microtubules in CC1-microinjected cells. In these cells, mEg5 on astral microtubules was nearly static, with a velocity of –0.34 nm/s, consistent with previous work in *Xenopus* extract spindles, which demonstrated that poleward transport of Eg5 in the half-spindle requires dynein–dynactin activity (Figure 7, B and C; Uteng *et al.*, 2008). On interzonal microtubules, the velocity of mEg5 punctae was not different from uninjected control cells (6.03 vs. 6.36 nm/s; Figure 7, B and C).

To determine further how Eg5 transport is regulated, we examined mEg5 behavior in cells depleted of the spindle-associated protein TPX2. TPX2 was first identified as a factor required for the dynein-dependent transport of the kinesin Xklp2 to spindle poles (Wittmann *et al.*, 1998) and has subsequently been shown to bind Eg5 and to contribute to the localization of the motor to spindle microtubules (Eckerdt *et al.*, 2008; Ma *et al.*, 2010, 2011). In TPX2-depleted cells, spindles are shortened and frequently multipolar (Figure 7A) and fail to progress through mitosis in a timely manner. We depleted TPX2 and examined mEg5 behavior on astral microtubules, which are retained in TPX2-depleted cells, and on midzone microtubules, which are present but somewhat shorter than in control cells. mEg5 on astral microtubules moved toward plus ends at a velocity of 6.93 nm/s and in some cases accumulated at microtubule tips (Figure 7, B and C). The velocity of mEg5 on astral microtubules in TPX2-depleted cells is lower than the plus end–directed velocity measured in anaphase cells (6.93 vs. 10.91 nm/s, respectively); this could result if some TPX2 remained in the cells after siRNA treatment or if Eg5 velocity is regulated by the cell cycle. On interzonal microtubules in TPX2-depleted cells, mEg5 velocity was not different from controls (6.03 vs. 6.10 nm/s). These results demonstrate that TPX2 is required for dynein-dependent poleward transport of Eg5 on astral microtubules and support the view that TPX2 links Eg5 to dynein/dynactin for poleward transport.

DISCUSSION

Transport of Eg5 on astral microtubules

Our analysis reveals several novel features of mEg5 on astral microtubules: first, motor activity changes from diffusion to short directed motion following nuclear envelope breakdown; second, the direction of motion changes from minus end–directed in early mitosis to plus end–directed in anaphase; and third, minus end–directed motion requires both dynein and TPX2 (Figure 7). Inhibition of dynein blocks directed mEg5 movement, whereas TPX2 depletion causes mEg5 movement to reverse its direction. Astral microtubules rarely interact with each other (Rusan and Wadsworth, 2005), indicating that motors likely move on tracks composed of one or a few microtubules.

The observation that the poleward motion of Eg5, a plus end–directed kinesin, requires dynein activity on astral microtubules is similar to the dynein-dependent, minus end–directed transport of Eg5 on half-zone microtubules in *Xenopus* extract spindles (Uteng *et al.*, 2008), indicating that motion of Eg5 on spindle and astral microtubules is similarly regulated. However, minus end–directed transport of Eg5 in the *Xenopus* half-spindle is faster (~50 nm/s) than what we detected on astral microtubules (~20 nm/s), a difference that could result from differences between astral and spindle microtubules, different regulation in meiotic vertebrate and mitotic mammalian spindles, and/or the method of measurement (photoactivation vs. particle tracking). The velocity of minus-end motion of Eg5 in both cases is slower than that of dynein/dynactin, which has been reported to move poleward at rates of 1–3 μm/s in the mammalian spindle and to move on microtubules in vitro at rates of ~75 nm/s for yeast dynein (Whyte *et al.*, 2008; Markus and Lee, 2011). The short dwell time we measured for Eg5 is also distinct from the processive motion of dynein (Schuster *et al.*, 2011). These results indicate that Eg5 on astral microtubules likely makes transient interactions with dynein/dynactin.

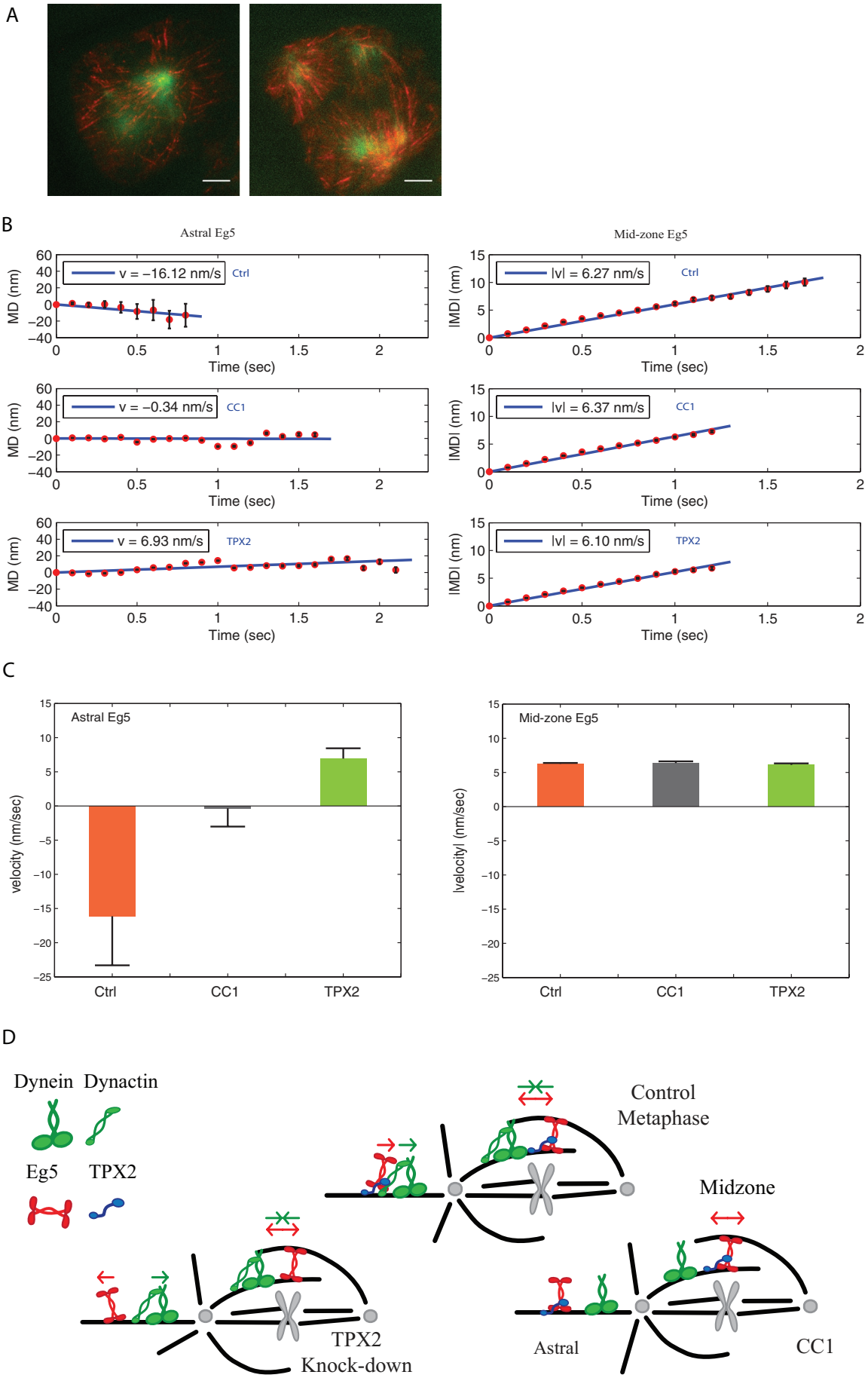
A
B
Astral Eg5
Mid-zone Eg5
v = −16.12 nm/s
Ctrl
|v| = 6.27 nm/s
v = −0.34 nm/s
CC1
|v| = 6.37 nm/s
v = 6.93 nm/s
TPX2
|v| = 6.10 nm/s
MD (nm)
|MD| (nm)
Time (sec)
C
velocity (nm/sec)
|velocity| (nm/sec)
Ctrl
CC1
TPX2
D
Dynein
Dynactin
Eg5
TPX2
Control
Metaphase
Midzone
TPX2
Knock-down
Astral
CC1

The velocity of plus end–directed motion of Eg5 in anaphase (~10 nm/s) is similar to the rate of individual Eg5 molecules moving on microtubules in vitro (8.5 nm/s; Weinger *et al.*, 2011), supporting the view that Eg5 punctae on astral microtubules are moving on individual microtubules. Plus-end motion of Eg5 was also detected in cells depleted of TPX2, indicating that TPX2 links Eg5 to dynein/dynactin for minus end–directed transport. The switch in the direction of Eg5 motion in anaphase suggests that the interactions among TPX2, Eg5, and dynein are temporally regulated to achieve spatial localization of Eg5. A candidate for this regulation is the small GTPase Ran, which has been demonstrated to alter motor activity on microtubule asters in *Xenopus* extracts (Wilde *et al.*, 2001).

Previous work has shown that purified Eg5 moves toward the plus ends of microtubules in vitro (Kapitein *et al.*, 2005; Weinger *et al.*, 2011). In contrast, Cin8p, a yeast kinesin-5 family member, switches the direction of motion in a manner that is dependent on the number of motors present on the microtubule (Roostalu *et al.*, 2011). Cin8p directionality is also regulated by ionic strength and the insert in loop 8 (Gerson-Gurwitz *et al.*, 2011). Our results demonstrate a change in the direction of Eg5 motion on astral microtubules in mammalian cells. In contrast to the situation in yeast, however, minus end–directed motion of Eg5 requires dynein/dynactin. These results explain the reorganization of Eg5 during mitosis, specifically the poleward enrichment of Eg5 during metaphase and the redistribution of Eg5 to spindle midzone during anaphase (Figure 2).

Eg5 behavior on antiparallel microtubules in the midzone

In the spindle midzone, in which microtubules are arranged in an antiparallel manner, Eg5 tetramers can engage two microtubules, leading to microtubule sliding (Kapitein *et al.*, 2005; van den Wildenberg *et al.*, 2008). Motion of Eg5 punctae in the midzone was similar throughout mitosis, and motion velocities were comparable in each direction. In prometaphase and metaphase, microtubules in the half-spindle and midzone of LLC-Pk1 cells undergo poleward flux (~23 nm/s); in anaphase cells, midzone microtubules do not show detectable flux (Figure S2B; Ferenz and Wadsworth, 2007; Ma *et al.*, 2010) indicating that the behavior of Eg5 is regulated independently of flux.

Depletion of TPX2 or inhibition of dynein did not alter the velocity of Eg5 punctae in the midzone. TPX2 and Eg5 both localize to midzone microtubules and the velocity of Eg5-dependent microtubule gliding and sliding in vitro is reduced by TPX2 (Ma *et al.*, 2011). One possibility is that TPX2 can reduce the velocity of microtubule motion without a detectable direct effect on the motion of Eg5. Dynein and Eg5 have been shown to generate antagonistic forces on antiparallel microtubules, but whether they interact directly at this location is not known. Our results show that inhibition of dynein shifts the distribution of Eg5, but does not directly alter motion of individual Eg5 punctae on midzone microtubules. Taken together these observations indicate that on antiparallel microtubules, Eg5 can simultaneously interact with two microtubules, and motion of the motor is restricted (Turner *et al.*, 2001).

A potential caveat of these experiments is that microtubule organization is altered following inhibition of dynein with CC1 and following depletion of TPX2. This could potentially impact motor behavior. However, we found that motor behavior on midzone and astral microtubules changed in discrete ways in the inhibited cells. Furthermore, our single-particle tracking was performed on individual microtubule filaments or bundles (see *Materials and Methods*) and thus did not require specific spindle morphology. Thus, we conclude that the changes we report are due to alterations in Eg5 behavior, not simply the result of disruption to microtubule organization.

We did not detect static motors on midzone microtubules, as was previously observed in the midzone using photoactivation (Uteng *et al.*, 2008) and throughout the *Xenopus* extract spindle using fluorescent speckle microscopy (Kapoor and Mitchison, 2001). One possible explanation for the difference is that similar brief, directed motion of kinesin-5 occurs in *Xenopus* spindles, but is not detected by photoactivation (Uteng *et al.*, 2008), which has a lower spatial–temporal resolution compared with single-particle tracking. For example, the half-life for kinesin-5 in the *Xenopus* midzone is ~19 s, whereas the dwell time measured on astral microtubules is very short. If motion occurs at ~50 nm/s, a large fraction of the motors would dissociate before moving outside of the photoactivation zone, which is the size of a few microns. Similarly, Eg5 behavior detected using wide-field fluorescent speckle microscopy (Kapoor and Mitchison, 2001) in cell extracts may differ from motions of Eg5 that we detected using TIRF and subpixel resolution particle-tracking in mammalian spindles.

Our results in mammalian cells support a model in which the mitotic functions of Eg5 are accomplished by individual motors making short, directed excursions along microtubules. At the velocities we measured and with an average dwell time of ~200 ms, each motor would move on average only a few nanometers each time before dissociation from the microtubule. We speculate that the collective action of many Eg5 motors, each interacting with the microtubule for a brief period, generates force in mitotic spindles. Such interactions may drive antiparallel microtubule sliding and dynamic cross-linking of parallel microtubules.

Conclusions

In summary, our results demonstrate that Eg5 localizes along spindle microtubules with an accumulation near spindle poles and relocalizes to the midzone in late anaphase. At a population level, Eg5 is highly dynamic in all spindle regions throughout mitosis. Individual Eg5 punctae in the spindle midzone are dynamic, not static, consistent with motor transient engagement on antiparallel microtubules. The direction of Eg5 movement on astral microtubules changes with the stage of mitosis. Our results support the view that cells deploy mitotic motors with high temporal and spatial precision to accomplish their mitotic function.

MATERIALS AND METHODS

Materials

Cell culture materials were obtained from either Sigma-Aldrich (St. Louis, MO) or Invitrogen Life Technologies (Carlsbad, CA), with the exception of fetal bovine serum (FBS), which was obtained from Atlanta Biologicals (Lawrenceville, GA). Mouse Eg5 BAC clone RP23-117H14 and BAC-cloning reagents were obtained from

FIGURE 7: Reorganization of Eg5 in the spindle requires dynein and TPX2. (A) Overlay of SD projection of time series of mEg5 in TIRF (red) and wide-field image of mEg5 (green) in a CC1-injected cell (right) or TPX2-depleted cell (left). (B) Mean displacement fitting to achieve the velocities of astral and midzone mEg5 punctae in controls and following inhibition of dynein or depletion of TPX2. Error bars show SE of the mean. (C) Bar plot of velocities of Eg5 punctae at different stages; velocities are plotted in mean ± 95% confidence interval of the estimated velocities. (D) Model showing motor behavior on astral and midzone microtubules in control, CC1-injected, and TPX2-depleted cells.

BACPAC Resources (Oakland, CA) and Gene Bridges (Heidelberg, Germany), respectively. Electroporation cuvettes were purchased from Molecular BioProducts (San Diego, CA). The C-terminal GFP-LAP tag (C-term R6K-Amp-LAP) was a gift from the laboratory of Anthony Hyman (Max Planck Institute, Dresden, Germany). Reagents used for mammalian transfection were obtained from Qiagen (Valencia, CA). Primary and secondary antibodies used for immunoblotting and immunofluorescence were obtained as follows: rabbit-anti-Eg5 (Novus Biologicals, Littleton, CO), goat anti-rabbit IgG Cy3, and goat anti–rabbit immunoglobulin G (IgG) horseradish peroxidase (HRP; Jackson ImmunoResearch Laboratories, West Grove, PA). S-agarose beads used for immunoprecipitation were a gift from Wei-Lih Lee (University of Massachusetts, Amherst, Amherst, MA). All other chemical reagents, unless specified, were obtained from Sigma-Aldrich (St. Louis, MO).

Cell culture

Pig kidney epithelial (LLC-Pk1) cells, and clones derived from these cells, were cultured in F10/OptiMEM with 7.5% FBS and antibiotics at 37°C in a 5% CO_2 atmosphere. For imaging, cells were plated at the appropriate density on glass coverslips 48–72 h prior to imaging.

BAC cloning

Mouse Eg5-BAC clone RP23-117H14 was received as a stab culture and was streaked onto lysogeny broth plates conditioned with chloramphenicol. Subsequent cloning steps were followed according to Gene Bridges' Counter-Selection BAC Modification Kit (Version 3.1, March 2008). Preparation of cells for electroporation was performed at 4°C and electroporation voltage was consistently 1.8 kV. Primers for C-terminal LAP-tagging and recombineering were designed based on primers from the Mitocheck BACPAC resources website (www.mitocheck.org/cgi-bin/BACfinder?query=eg5&query_type=mouse&species=mouse). mEg5-LAP–tagged BAC DNA was purified by following NucleoBond BAC 100 (Clontech, Mountain View, CA) maxiprep protocol.

Mammalian transfection and Western analysis

LLC-Pk1 cells were plated at a density of 1.0×10^5 and after 48 h were transfected with mouse Eg5-LAP–tagged BAC using Effectene at a 1:25 ratio of DNA to transfection reagent. Transfected cells were selected in 2.0 g/l G418 for 2 wk. Whole-cell extracts were prepared by lysis in 0.5% SDS, 1 mM EDTA, and the protease inhibitors aprotinin (0.02 mg/ml), leupeptin (0.01 μg/ml), and Pefabloc (0.1 mg/ml), and then sonicated twice for 10 s, with cooling in between sonications. A sample was saved for Lowry protein determination and extracts were boiled for 5 min after the addition of 6× SDS sample buffer. Extracts were run on an 8% polyacrylamide gel and then transferred to Amersham Hybond-P membrane (GE Healthcare, Waukesha, WI). Blots were probed with a rabbit anti-Eg5 antibody (1:1000) for 1 h at room temperature and goat anti-rabbit IgG HRP-tagged secondary antibody (1:5000) for 1 h at room temperature. Blots were detected using chemiluminescence.

Inhibition of dynein and siRNA depletion of TPX2

To inhibit the dynein–dynactin interaction, cells were microinjected with the CC1 fragment of p150. Needle concentration of CC1 was 1.6 mg/ml. The CC1 fragment of p150 was expressed and purified from *Escherichia coli* BL21(DE3)pLysS by ammonium sulfate precipitation and high-salt boiling (King *et al.*, 2003; Ferenz *et al.*, 2009). Purified p150 CC1 was dialyzed into microinjection buffer (50 mM sodium glutamate, pH 7.2). To deplete endogenous pig TPX2, we used the sequence GAAUGGUACAGGAGGCUU (Tulu *et al.*, 2006). For transfection, 1.5×10^5 cells were plated per coverslip and were transfected using Oligofectamine (Invitrogen). The final concentration of siRNA used was 20 nM. Four hours after the siRNA complexes were added, cells were transferred to complete medium and examined 40 h following transfection.

mEg5 pulldown using S-peptide

LLC-Pk1 mEg5 cells were treated with 100 nM nocodazole ~20 h prior to preparation of cell extracts. Whole-cell extracts were prepared as follows: cells were lysed in 50 mM HEPES, 150 mM NaCl, 1% NP-40, and protease inhibitors (aprotinin [0.04 mg/ml], leupeptin [0.02 μg/ml], and Pefabloc [0.2 mg/ml]). Lysates were incubated on ice for 10 min with agitation at 5 min and spun at top speed in a microcentrifuge for 30 min at 4°C. The supernatant was stored on ice. S-agarose beads were washed with lysis buffer, and the lysate was added to the washed S-agarose beads. The complex was incubated for 1 h at 4°C with rotation. After incubation, the complex was spun down, and the beads were washed with lysis buffer and centrifuged. Beads were resuspended in SDS sample buffer and boiled for 3 min. SDS–PAGE and immunoblotting were performed as described in the *Mammalian transfection and Western analysis* section.

Immunofluorescence

LLC-Pk1 mEg5 cells were plated on coverslips and fixed 72 h later. Cells were lysed in extraction buffer (80 mM PIPES, pH 6.9, 5 mM EGTA, 1 mM $MgSO_4$, and 0.5% TritonX-100) for 8 s, fixed in 100% MeOH on ice, and rehydrated in PBS-Tween-Azide. Cells were stained for Eg5 using rabbit anti-Eg5 primary antibody (1:1000) for 1 h at 37°C and secondary antibody goat anti–rabbit Cy3 (1:200) for 1 h at room temperature. Coverslips were mounted on glass slides using Vectashield mounting medium (Vector Laboratories, Burlingame, CA) and sealed with nail polish.

Microscopy

Cells fixed and stained for Eg5 were observed and imaged as previously described (Rusan *et al.*, 2001; Ferenz *et al.*, 2009). Live-cell imaging was performed using a Zeiss (Carl Zeiss MicroImaging, Thornwood, NY) LSM 510 Meta laser-scanning confocal unit on an Axiovert 200 microscope equipped with a 63×, 1.4 numerical aperture objective lens. Images were acquired at 488-nm excitation using LSM software with a unidirectional scan speed of 8 and a scan number of 8. All imaging was performed at 37°C in a Tempcontrol 37-2 digital environmental chamber. Photoactivation of cells expressing photoactivatible-GFP-tubulin was performed as previously described (Ma *et al.*, 2010). Live-cell imaging was also performed using a spinning-disk confocal (PerkinElmer-Cetus, Waltham, MA) on a Nikon TE300 microscope. To quantify the levels of Eg5 and tubulin, fluorescence of Eg5 and tubulin was measured at the midzone and near the spindle pole. The ratio of Eg5 signal to tubulin signal was determined, and the fold enrichment of Eg5 at spindle poles was calculated. Fluorescence measurements, which were corrected for background, were made using MetaMorph software. To determine the contribution of dynein to Eg5 localization, fluorescence of tubulin and Eg5 were measured in the half-spindle prior to microinjection of CC1 and after microinjection. The preinjection Eg5 to microtubule ratio was set to 100%.

FRAP experiments and data analysis

LLC-Pk1 mEg5 cells were imaged for three frames, and then the fluorescence was bleached with 75 iterations of 100% 488-nm laser light in a region ranging from ~2×2 to ~5×5 μm and subsequently imaged every 1.18 s for a total of 60 s. Scan speed was set

at a maximum value of 11 with a scan number of 4. Bleach regions were placed around the centrosome in prophase cells; in the half-spindle for prometaphase, metaphase, and early anaphase cells; and at the midzone between the separating chromosomes in late anaphase. During experiments, cells were maintained in an environmental chamber held constant at 37°C. For Taxol treatment, cells were treated with 100 nM placitaxel prior to imaging. For measurement of tubulin FRAP, LLC-Pk1 cells expressing GFP-α-tubulin were used.

Eg5 FRAP analysis was performed using ImageJ software (National Institutes of Health, Bethesda, MD) and KaleidaGraph (Synergy Software, Reading, PA). All FRAP time-lapse sequences were corrected for spindle movement using the StackReg (rigid body) plug-in for ImageJ. Aside from the bleach region of interest (ROI) two other ROIs of the same size were used: one for background subtraction and the other for photobleaching correction. The mean fluorescence intensity for each ROI throughout the time-lapse sequence was calculated by ImageJ and imported into an Excel (Microsoft Office 2007, Redmond, WA) worksheet. Fluorescence intensities were corrected for photobleaching, background-subtracted, and normalized so that the fluorescence intensity prebleach was 1 a.u. These values were plotted against time in KaleidaGraph and were fit to a single exponential curve. The results of this analysis are consistent with previous measurements of tubulin dynamics made using photoactivation (Zhai *et al.*, 1996; Cimini *et al.*, 2006) and FRAP (Saxton *et al.*, 1984; Wadsworth and Salmon, 1986).

TIRF microscopy

TIRF microscopy was performed using a customized system. The microscope, a Nikon Ti-E microscope with a 60×, 1.4 numerical aperture objective, has an Intenselite XeHg light source and light guide for illumination in the epifluorescence path and dichroic cubes for visualization in blue, green, and red wavelengths. In addition, there are another two sets of dichroic cubes for TIRF illumination. Lasers for TIRF include a green diode laser (532 nm, 100 mW) and a blue diode laser (488 nm, 50 mW). The system is run by Nikon Elements software. Images were acquired using a Cascade II 512 × 512 pixel camera. A 4× image expansion telescope was placed in front of the camera. To visualize mEg5 movement, a time-lapse movie was acquired in TIRF using a 100-ms exposure with no shutter delay. The SD of the intensity of each pixel was calculated using ImageJ (Zprojection_StandardDeviation; Cai *et al.*, 2007).

For Eg5 inhibition experiments, cells were treated with 10 μM STLC, which was followed by a 2-h incubation prior to imaging. For microtubule depolymerization experiments, 10 μM nocodazole was added to cells expressing mEg5. During imaging, cells were maintained in non-CO_2 MEM pretreated with 0.3 U/ml Oxyrase oxygen-scavenging system (EC Oxyrase; Oxyrase, Mansfield, OH).

Automated single-particle tracking

Automated single-particle tracking of mEg5 punctae was performed as in Yang *et al.* (2008), with minor modifications using customized software implemented in MATLAB (MathWorks, Natick, MA). Specifically, to identify locations of different microtubules or microtubule bundles, all frames from a time-lapse movie were first added up to generate a sum image, in which individual microtubules or microtubule bundles manifested as bright-intensity bands. Then, locations of individual microtubules or microtubule bundles were determined by manually tracing the centerline (skeleton) of each intensity band. After the centerline of each microtubule or microtubule bundle was defined, a morphological dilation process was performed to generate an ROI of two pixels in width from each side of the microtubule centerline (Snyder and Qi, 2004). Fluorescent particle detection and tracking were carried out subsequently only in defined ROIs. First, individual mEg5 punctae were detected, as in Yang *et al.* (2008). Then, intensity profiles of individual punctae were fit by a two-dimensional Gaussian model to achieve subpixel resolution. Trajectories of individual punctae along microtubules were recovered by single-particle tracking (Yang *et al.*, 2008). Detected trajectories of individual mEg5 punctae were projected onto the directions of their associated microtubules for calculation of net displacement. Robust least-square regression was applied to fit the mean displacement versus time data to extract velocity information (for linear regression analysis, see Seber 2003). When averaging velocities of mEg5 punctae over the movies collected for the same stage of mitosis, we determined the polarity of each astral microtubule or microtubule bundle manually, based on visual inspection. For interzonal microtubules, only the magnitude of displacement was analyzed without differentiating underlying microtubule polarities.

The dwell time of each puncta was calculated according to the length of its trajectory. Since the time-lapse movie was taken at 10 frames per second, the shortest resolved time step is 100 ms. In all cases, the majority of punctae had dwell times <200 ms, and <5% of punctae were associated with microtubules for longer than 400 ms. For astral Eg5, statistics were obtained from recovered trajectories: 13,572 trajectories from four cells at prophase, 591 trajectories from two cells at prometaphase, 2801 trajectories from four cells at metaphase, 12,720 trajectories from eight cells at early anaphase, and 10,218 trajectories from four cells at late anaphase. For midzone Eg5, data were collected from 6486 trajectories from six cells at prometaphase, 20,343 trajectories from 15 cells at metaphase, 12,761 trajectories from nine cells at early anaphase, and 7803 trajectories from four cells at late anaphase (see Supplemental Table S1).

ACKNOWLEDGMENTS

The authors are especially indebted to Ina Poser and Alex Bird (Hyman laboratory, Dresden, Germany) for their generous assistance with many aspects of BACs and recombineering and for reagents. We thank Wei-Lih Lee and members of his laboratory for generosity with reagents and equipment. We thank members of the Ross laboratory for assistance with TIRF microscopy; Raja Ghosh, David Gross, and Dale Callaham for assistance with FRAP; and Katherine Dorfman for assistance with statistics. We thank Thomas Maresca and Wei-Lih Lee for comments on the manuscript. M.Q. is supported by a Dowd–ICES fellowship; G.Y. is supported by National Science Foundation (NSF) grants MCB-1052660 and DBI-1052925, and P.W. is supported by NSF DBI-0923318.

REFERENCES

Amin-Hanjani S, Wadsworth P (1991). Inhibition of spindle elongation by taxol. Cell Motil Cytoskeleton 20, 136–144.

Bannigan A, Scheible W, Lukowitz W, Fagerstrom C, Wadsworth P, Somerville C, Baskin TI (2007). A conserved role for kinesin-5 in plant mitosis. J Cell Sci 120, 1–6.

Blangy A, Arnaud L, Nigg EA (1997). Phosphorylation by $p34^{cdc2}$ protein kinase regulates binding of the kinesin related motor HsEg5 to the dynactin subunit $p150^{glued}$. J Biol Chem 272, 19418–19424.

Blangy A, Lane HA, d'Herin P, Harper M, Kress M, Nigg EA (1995). Phosphorylation by $p34^{cdc2}$ regulates spindle association of human Eg5, a kinesin related motor essential for bipolar spindle formation in vivo. Cell 83, 1159–1169.

Cahu J, Olichon A, Hentrich C, Schek H, Drinjakovic J, Zhang C, Doherty-Kirby A, Lajoie G, Surrey T (2008). Phosphorylation by Cdk1 increases the binding of Eg5 to microtubules *in vitro* and in *Xenopus* egg extract spindles. PLoS One 3, e3936.

Cai D, Verhey KJ, Meyhofer E (2007). Tracking single kinesin molecules in the cytoplasm of mammalian cells. Biophys J 92, 4137–4144.

Cheerambathur DK, Brust-Mascher I, Civelekoglu-Scholey G, Scholey JM (2008). Dynamic partitioning of mitotic kinesin-5 cross-linkers

between microtubule-bound and freely diffusing states. J Cell Biol 182, 429–436.
Cheeseman IM, Desai A (2005). A combined approach for the localization and tandem affinity purification of protein complexes from metazoans. Sci STKE 2005, 11.
Cimini D, Wan X, Hirel CB, Salmon ED (2006). Aurora kinase promotes turnover of kinetochore microtubules to reduce chromosome segregation errors. Curr Biol 16, 1711–1718.
Cole DG, Saxton WM, Sheehan KB, Scholey JM (1994). A "slow" homotetrameric kinesin-related motor protein purified from *Drosophila* embryos. J Biol Chem 269, 22913–22916.
Eckerdt F, Eyers PA, Lewellyn AL, Prigent C, Maller JL (2008). Spindle pole regulation by a discrete Eg5-interacting domain in TPX2. Curr Biol 18, 519–525.
Ferenz N, Paul R, Fagerstrom C, Mogilner A, Wadsworth P (2009). Dynein antagonizes Eg5 by crosslinking and sliding antiparallel microtubules. Curr Biol 19, 1833–1838.
Ferenz NP, Gable A, Wadsworth P (2010). Mitotic functions of kinesin-5. Semin Cell Dev Biol 21, 255–259.
Ferenz NP, Wadsworth P (2007). Prophase microtubule arrays undergo flux-like behavior in mammalian cells. Mol Biol Cell 18, 3993–4002.
Gerson-Gurwitz A, Thiede C, Movshovich N, Fridman V, Podolskaya M, Danieli T, Lakämper S, Klopfenstein DR, Schmidt CF, Gherber L (2011). Directionality of individual kinesin-5 Cin8 motors is modulated by loop 8, ionic strength and microtubule geometry. EMBO J 30, 4942–4954.
Heck MMS, Pereira A, Pesavento P, Yannoni Y, Spradling AC, Goldstein LSB (1993). The kinesin-like protein KLP61F is essential for mitosis in *Drosophila*. J Cell Biol 123, 665–679.
Hoyt MA, He L, Loo KK, Saunders WS (1992). Two *Saccharomyces cerevisiae* kinesin-related gene products required for mitotic spindle assembly. J Cell Biol 118, 109–120.
Kapitein LC, Peterman EJG, Kwok BH, Kim JH, Kapoor TM, Schmidt CF (2005). The bipolar mitotic kinesin Eg5 moves on both microtubules that it crosslinks. Nature 435, 114–118.
Kapoor T, Mitchison TJ (2001). Eg5 is static in bipolar spindles relative to tubulin: evidence for a static spindle matrix. J Cell Biol 154, 1125–1133.
Kashina AS, Baskin RJ, Cle DG, Wedaman KP, Saxton WM, Scholey JM (1996). A bipolar kinesin. Nature 379, 270–272.
King SJ, Brown CL, Maier KC, Quintyne NJ, Schroer TA (2003). Analysis of the dynein-dynactin interaction in vitro and in vivo. Mol Biol Cell 14, 5089–5097.
Kittler R, Pelletier L, Ma C, Poser I, Fisher S, Hyman AA, Buchholz F (2005). RNA interference rescue by bacterial artificial chromosome transgenesis in mammalian tissue culture cells. Proc Natl Acad Sci USA 102, 2396–2401.
Korneev MJ, Lakamper S, Schmidt CF (2007). Load-dependent release limits the processive stepping of the tetrameric Eg5 motor. Eur Biophys J 36, 675–681.
Kwok BH, Kapitein LC, Kim JH, Peterman EJG, Schmidt CF, Kapoor TM (2006). Allosteric inhibition of kinesin-5 modulates its processive directional motility. Nat Chem Biol 2, 480–485.
Le Guellec R, Paris J, Couturier A, Roghi C, Phillipe M (1991). Cloning by differential screening of a *Xenopus* cDNA that encodes a kinesin-related protein. Mol Cell Biol 11, 3395–3398.
Ma N, Titus J, Gable A, Ross JL, Wadsworth P (2011). TPX2 regulates the localization and activity of Eg5 in the mammalian mitotic spindle. J Cell Biol 195, 87–98.
Ma N, Tulu S, Ferenz N, Fagerstrom C, Wilde A, Wadsworth P (2010). Poleward transport of TPX2 in mammalian spindles requires Eg5, dynein and microtubule flux. Mol Biol Cell 21, 979–988.
Markus SM, Lee W-L (2011). Regulated offloading of cytoplasmic dynein from microtubule plus ends to the cortex. Dev Cell 20, 639–651.
Mastronarde DN, McDonald KL, Ding R, McIntosh JR (1993). Interpolar spindle microtubules in PtK cells. J Cell Biol 123, 1475–1489.
Mayer TU, Kapoor TM, Haggarty SJ, King RW, Schreiber SL, Mitchison TJ (1999). Small molecule inhibitor of mitotic spindle bipolarity identified in a phenotype-based screen. Science 286, 971–974.
Poser I *et al*. (2008). BAC transgeneOmics: a high-throughput method for exploration of protein function in mammals. Nat Methods 5, 409–415.
Quintyne NJ, Gill SR, Eckley DM, Crego CL, Compton DA, Schroer TA (1999). Dynactin is required for microtubule anchoring at fibroblast centrosomes. J Cell Biol 147, 321–334.
Reddy AS, Day IS (2001). Kinesin in the Arabidopsis genome: a comparative analysis among eukaryotes. BMC Genomics 2, 2–14.
Roof DM, Meluh PB, Rose MD (1992). Kinesin-related proteins required for the assembly of the mitotic spindle. J Cell Biol 118, 95–108.
Roostalu J, Hentrich C, Bieling P, Telley IA, Schiebel E, Surrey T (2011). Directional switching of the kinesin Cin8 through motor coupling. Science 332, 94–99.
Rusan NM, Fagerstrom C, Yvon AC, Wadsworth P (2001). Cell cycle dependent changes in microtubule dynamics in living cells expressing GFP-alpha tubulin. Mol Biol Cell 12, 971–980.
Rusan NM, Wadsworth P (2005). Centrosome fragments and microtubules are released and transported asymmetrically away from division plane in anaphase. J Cell Biol 168, 21–28.
Saunders WS, Hoyt MA (1992). Kinesin-related proteins required for the structural integrity of the mitotic spindle. Cell 70, 451–458.
Sawin KE, LeGuellec K, Philippe M, Mitchison TJ (1992). Mitotic spindle organization by a plus-end directed microtubule motor. Nature 359, 540–543.
Sawin KE, Mitchison TJ (1995). Mutations in the kinesin-like protein Eg5 disrupting localization to the mitotic spindle. Proc Natl Acad Sci USA 92, 4289–4293.
Saxton WM, Stemple DL, Leslie RJ, Salmon ED, Zavortink M, McIntosh JR (1984). Tubulin dynamics in cultured mammalian cells. J Cell Biol 99, 2175–2186.
Schuster M, Lipowsky R, Assmann M-A, Lenz P, Steinberg G (2011). Transient binding of dynein controls bidirectional long-range motility of early endosomes. Proc Natl Acad Sci USA 108, 3618–3623.
Seber GAF (2003). Linear Regression Analysis, 2nd ed, Hoboken, NJ: John Wiley & Sons.
Sharp DJ, McDonald KL, Brown HM, Matthies HJ, Walczak CE, Vale RD, Mitchison TJ, Scholey JM (1999). The bipolar kinesin, KLP61F, cross-links microtubule within interpolar microtubule bundles of *Drosophila* embryonic mitotic spindles. J Cell Biol 144, 125–138.
Snyder WE, Qi H (2004). Machine Vision, New York: Cambridge University Press.
Tanenbaum ME, Macurek L, Galjart N, Medema RH (2008). Dynein, Lis1 and CLIP170 counteract Eg5-dependent centrosome separation during bipolar spindle assembly. EMBO J 27, 3235–3245.
Tsai M-Y, Wang S, Heidinger JM, Shumaker DK, Adam SA, Goldman RD, Zheng X (2006). A mitotic lamin B matrix induced by RanGTP required for spindle assembly. Science 311, 1887–1893.
Tulu US, Rusan NM, Fagerstrom C, Ferenz NP, Wadsworth P (2006). Molecular requirements for kinetochore-associated microtubule formation in mammalian cells. Curr Biol 16, 536–541.
Turner J, Anderson R, Guo J, Beraud C, Fletterick R, Sakowicz R (2001). Crystal structure of the mitotic spindle kinesin Eg5 reveals a novel conformation of the neck-linker. J Biol Chem 276, 25496–25502.
Uteng M, Hentrich C, Bieling P, Surrey T (2008). Poleward transport of Eg5 by dynein-dynactin in *Xenopus* egg extract spindles. J Cell Biol 182, 715–726.
van den Wildenberg SMJL, Tao L, Kapitein LC, Schmidt CF, Scholey JM, Peterman EJG (2008). The homotetrameric kinesin-5 KLP61F preferentially crosslinks microtubules into antiparallel orientations. Curr Biol 18, 1860–1864.
Vanneste D, Takagi M, Imamoto N, Vernos I (2009). The role of Hklp2 in the stabilization and maintenance of spindle bipolarity. Curr Biol 19, 1712–1717.
Wadsworth P, Salmon ED (1986). Analysis of the treadmilling model during metaphase of mitosis using fluorescence recovery after photobleaching. J Cell Biol 102, 1032–1038.
Weinger JS, Qiu M, Yang G, Kapoor TM (2011). A nonmotor microtubule binding site in kinesin-5 is required for filament crosslinking and sliding. Curr Biol 21, 154–160.
Whyte J *et al*. (2008). Phosphorylation regulates targeting of cytoplasmic dynein to kinetochores during mitosis. J Cell Biol 183, 819–834.
Wilde A, Lizarraga SB, Zhang L, Wiese C, Glicksman NR, Walczak CE, Zheng Y (2001). Ran stimulates spindle assembly by altering microtubule dynamics and the balance of motor activities. Nat Cell Biol 3, 221–227.
Wittmann T, Boleti H, Antony C, Karsenti E, Vernos I (1998). Localization of the kinesin-like protein Xklp2 to spindle poles requires a leucine zipper, a microtubule-associated protein and dynein. J Cell Biol 143, 673–685.
Yang G, Cameron LA, Maddox PS, Salmon ED, Danuser G (2008). Regional variation of microtubule flux reveals microtubule organization in the metaphase spindle. J Cell Biol 182, 631–639.
Yvon AC, Wadsworth P, Jordan MA (1999). Taxol suppresses dynamics of individual microtubules in living human tumor cells. Mol Biol Cell 10, 947–959.
Zhai Y, Kronebusch RJ, Simon PM, Borisy GG (1996). Microtubule dynamics at the G2/M transition: abrupt breakdown of cytoplasmic microtubules at nuclear envelope breakdown and implications for spindle morphogenesis. J Cell Biol 135, 201–214.